Modelling and Parametric Study for Panel Flutter Problem using Functionally Graded Materials

Journal of Physics: Conference Series **2811** (2024) 012030 doi:10.1088/1742-6596/2811/1/012030

Modelling and Parametric Study for Panel Flutter Problem using Functionally Graded Materials

Mohamed E Fayed [1*], Mourad S Semary [1], A A El Desouky [1], Ehab Ali [1], and Mohammad Tawfik [2,3]

[1] Basic Engineering Sciences Department, Benha Faculty of Engineering, Benha University, Egypt.
[2] Academy of Knowledge, Cairo, Egypt.
[3] United Arab Emirates University, UAE.

*Corresponding author's email: melsayed@bhit.bu.edu.eg

Abstract. In this paper we will demonstrate the possibility of weight optimization of panels under aero-thermal loading in hypersonic flow using functionally graded materials (FGM). The in-plane volume fraction of two constituents (Aluminium and Nickel) is modelled using polynomial distributions. Different material grading layouts are investigated, including cases with Nickel concentrated at corners, sides, midpoints and center. The solution of the problem utilized a higher order element with C^1 continuity. The study covers the linear boundaries of the panel flutter problem as well as the non-linear post-buckling deflections. The results indicated Nickel placement strategies are shown to enhance dynamic pressure and vibration performance for a given mass reduction through optimal center and edge localization. Overall, the integrated modelling approach demonstrates the potential to systematically optimize stability, weight and integrity in hypersonic flow to optimize the weight of panels subject to aero-thermal loads.

1. Introduction

In the dynamic world of aerospace engineering, the pursuit of optimal structures is an ongoing challenge. This paper delves into the interplay of materials and aerodynamics, aiming to reduce the instability of thin plates with minimal weight increase. Multifunctional structures in next-generation aerospace vehicles operate in extreme environments, necessitating stability and control advances. Recent studies across formulations, experiments, computations, and investigations into underlying mechanisms contribute understanding across the domains of modeling methodologies, passive stabilization concepts, benchmark validation efforts, active control strategies, and fundamental instability mechanisms.

An extensive research effort has focused recently on theoretically and numerically analyzing stability and flutter phenomena in panels under aerodynamic, thermal, acoustic and multifunctional loads to enable optimization. [1] developed finite element modeling to evaluate the effects of functionally graded materials and constituents on thermal buckling and nonlinear flutter in panels, finding silicon nitride-Nickel reinforcement improves temperature-dependent response while spatial gradations and mixing ratios significantly influence static and dynamic behavior. [2] established related formulation specialized for efficient flutter and buckling analysis, where Nickel-silicon nitride blending tunes stability and graded variations optimize integrity, vibrations and aerodynamic performance.

[3] put forward symbolic derivatives and optimization for variability quantification in free vibration of functionally graded plates, demonstrating higher-order reliability methods agree well with Monte Carlo

simulations. The approach provides a basis to extend robustness-based design optimization to multiple performance metrics leveraging graded materials. [4] focused on thermal flutter in graded panels, determining increased ceramic volume fraction elevates flutter resistance as well as high-cycle fatigue driving loads. Studies [5, 6] explored nonlinear finite element analysis and time-domain simulations to reveal complex trade-offs between post-buckling, forced response and fatigue life predictions under combined thermal-acoustic loads. Researches [7-10] developed and validate iso-geometric, meshless and consistent thickness plate theories for efficient and accurate modeling of stability in functionally graded structures under thermal and mechanical loads. Analyses show the approaches efficiently optimize material distribution to reduce peak stress and mass while improving computational performance. [11-14] put forward plate formulations specialized for stability and vibration analysis in rotating blades, porous sandwich composites and bi-directionally graded materials using shear and thickness deformation assumptions. [15] derived analytical flutter solutions for porous functionally graded plates to quantify porosity effects on frequencies and speed, enabling design optimization. [16] found stability highly sensitive to integrated mass and stiffness elements, motivating passive flutter suppression concepts. [17] proposed and analyzes embedded nonlinear vibration absorbers to improve panel flutter boundaries, where distributed absorbers avoid position optimization and provide significant vibration mitigation invariant of pressure and airflow. [18] developed modeling to capture thermal effects and thickness variations on supersonic blade flutter, determining high temperatures and tapered geometry reduce stability.

[19] studied post-buckling and flutter behaviors of reinforced composite cylindrical panels under combined thermal-aerodynamic loads using a shear deformation formulation, concluding pressure and temperature diminish flutter resistance. [20] established multifunctional modeling and control of panel flutter stability in piezoelectric functionally graded materials under joint thermal-electrical-aerodynamic loads, where actuation authority improves but degrades at elevated temperatures. [21] highlighted the aeroelastic tailoring potential of graphene platelet reinforcement in graded Aluminium panels to simultaneously enhance structural and aerodynamic metrics. [22] found stability and vibration response of sandwich plates with porous cores depends on foundation interactions and internal material tailoring provides optimization opportunities. Pioneer research [23] developed multi physics modelling of porous nanocomposite cylinders with graphene fillers to quantify thermal buckling and vibrational impacts from porosity distributions and Nano reinforcements. The collective efforts advance understanding of stability in emerging aerospace structures to balance competing objectives through systematically tailored multifunctional gradations.

The extensive efforts on stability modeling and analysis have enabled significant progress in quantifying and optimizing the multifunctional performance of graded panels under aeroelastic, thermomechanical and acoustoelastic loads. The presented studies have established and validated efficient formulations specialized for tailored stability and vibrational evaluations using higher-order plate theories, advanced solutions approach and reliability methods. The investigations have provided detailed characterization of static, dynamic and post-buckling behavior in emerging graded structures based on constituent mixing ratios, porosities, anisotropic reinforcements and spatial property gradations. The modeling capabilities demonstrate the potential to balance metrics like strength, fluctuations, aerodynamics, and thermal resilience in next-generation adaptive structures through systematic tailoring of material and geometric gradients.

To the extent of the authors' knowledge, previous studies have not examined functionally graded plates from the perspective of the in-plane volume fraction optimization. In this paper we investigated the possibility of weight optimization of the panel using polynomial distribution of volume fraction(VF) of two materials (Aluminium and Nickel) in the plain of the plate.

2. Finite Element Formulation of Thermal Post-buckling of FGMs Panels

The equations governing the motion, considering large deflection and material properties, are formulated for a functionally graded plate exposed to aerodynamic and thermal loads. In order to accurately model the bending behaviour of the plate with material property variations, a single five-node quadrilateral element with C^1 continuity of deflections and slopes is utilized [24]. Using this element avoided ill-conditioning issues that can occur with higher order Lagrangian shape functions.

2.1. Nonlinear Strain-Displacement Relation

The in-plane strains and curvatures, based on the von Kármán moderately large deflection, are given by:

$$\begin{Bmatrix}\epsilon_x\\ \epsilon_y\\ \gamma_{xy}\end{Bmatrix}=\begin{Bmatrix}u_x\\ v_y\\ u_y+v_x\end{Bmatrix}+\frac{1}{2}\begin{Bmatrix}w_x^2\\ w_y^2\\ 2w_xw_y\end{Bmatrix}-z\begin{Bmatrix}w_{xx}\\ w_{yy}\\ 2w_{xy}\end{Bmatrix} \tag{1}$$

or, in compact form,

$$\{\epsilon\}=\{\epsilon_m\}+\frac{1}{2}\{\epsilon_\theta\}+\{\epsilon_b\} \tag{2}$$

Where:$\{\varepsilon_m\}$ is the membrane linear strain vector, $\{\varepsilon_\theta\}$ is the membrane nonlinear strain vector, $\{\varepsilon_b\}$ is the bending strain vector, $\{u,v\}$ are the in-plane displacements and $\{w,w_x,w_y,w_{xy}\}$ are the transverse displacements.

2.2. Stress–Strain Relationship of an FGMs Panel

The stress–strain relations for material that has changing properties in the x and y-directions can be expressed as follows:

$$\{\sigma\}=\begin{Bmatrix}\sigma_x\\ \sigma_y\\ \tau_{xy}\end{Bmatrix}=[Q(x,y)]\{\varepsilon\} \tag{3}$$

Where: $\{\sigma\}$ is the in-plane stress vector, $[Q(x,y)]$ is the stiffness matrix. The equilibrium relations may be expressed as:

$$\begin{Bmatrix}N\\ M\end{Bmatrix}=\begin{bmatrix}[A] & [0]\\ [0] & [D]\end{bmatrix}\begin{Bmatrix}\varepsilon\\ \kappa\end{Bmatrix}-\begin{Bmatrix}\begin{Bmatrix}N_T\\ M_T\end{Bmatrix}\end{Bmatrix} \tag{4}$$

Where:

$$([A],[D])=\iint_A\ [Q(x,y)](1,z^2)dz$$

$$[\mathrm{Q}(x,y)]=\begin{bmatrix}\dfrac{E(x,y)}{1-\nu^2(x,y)} & \dfrac{\nu(x,y)E(x,y)}{1-\nu^2(x,y)} & 0\\ \dfrac{\nu(x,y)E(x,y)}{1-\nu^2(x,y)} & \dfrac{E(x,y)}{1-\nu^2(x,y)} & 0\\ 0 & 0 & \dfrac{E(x,y)}{2[1+\nu(x,y)]}\end{bmatrix}$$

Where: $[A],[D]$ are the stiffness matrices, $\{N\},\{M\}$ are the resultant vectors of the in-plane force, moment $\{N_T\},\{M_T\}$ are the in-plane thermal load and thermal bending moment, E is the modulus of elasticity and ν is the Poisson ratio.

2.3. Aerodynamic Loading

The first-order quasi-steady piston theory for supersonic flow states that:

$$P_a=-\left(\frac{g_a}{\omega_0}\frac{D_{11}}{a^4}\frac{\partial w}{\partial t}+\lambda\frac{D_{11}}{a^3}\frac{\partial w}{\partial x}\right) \tag{5}$$

With

$$\mathrm{q}=\rho V^2/2\,,\quad \beta=\sqrt{M_\infty^2-1},\quad g_a=\frac{\rho_a V(M_\infty^2-2)}{\rho h\omega_0\beta^3},\qquad \lambda=\frac{2qa^3}{\beta D_{11}},\qquad \omega_o=\left(\frac{D_{11}}{\rho h a^4}\right)^{\frac{1}{2}}$$

$$D_{11} = \frac{Eh^3}{12(1-\nu^2)}$$

Where: P_a is the aerodynamic loading. V is the velocity of airflow. $M\infty$ is the Mach number. q is the dynamic pressure. ρa is the air mass density. g_a is non-dimensional aerodynamic damping. λ is non-dimensional aerodynamic pressure. D_{11} is the first entry of the flexural stiffness matrix $[D]$. a is the panel length in the flow direction, ω_0 is the frequency and β is the solidity ratio.

2.4. Equation of motion

The equation of motion for functionally graded material involves predicting both the buckling response and post-buckling deformations. As outlined by [25], this entails a multi-step process using the finite element method. This direct coupled approach between linear buckling and geometrically nonlinear post-buckling analysis provides an efficient simulation procedure for resolving panel can be obtained as:

$$[M]\{\ddot{W}\} + [G]\{\dot{W}\} + ([K] - [K_T] + \lambda[A_a] + \frac{1}{2}[N_1] + \frac{1}{3}[N_2])\{W\} = \{P_T\} \quad (6)$$

Where: $[M]$ is the mass matrix, $[G]$ is the aerodynamic damping matrix, $[K]$ is the linear stiffness matrix, $[K_T]$ is the thermal geometric stiffness matrix, $[A_a]$ is the aerodynamic stiffness, $[N_1]$ is the first order nonlinear stiffness matrix and $[N_2]$ is the second order nonlinear stiffness matrix.

Separating equations (6) into lateral and transverse directions, we obtain the following two equations.

$$[M_b]\{\ddot{W}_b\} + \frac{g_a}{\omega_0}[G]\{\dot{W}_b\} + \left[[K_b] - [K_T] + \frac{\lambda}{a^3}[A_a] + \frac{1}{2}[N1_{nm}] + \frac{1}{3}[N2_b]\right]\{W_b\} = \{P_{b\Delta T}\} + \{P_b(t)\} \quad (7)$$

$$[M_m]\{\ddot{W}_m\} + [K_m]\{W_m\} = \{P_{m\Delta T}\} \quad (8)$$

Where: suffixes b, m and nm, are the bending, membrane and the nonlinear terms.

$\{P_b(t)\}$ is the external load vector, $\{P_{b\Delta T}\}$ } is the thermal load vector.

2.5. Static Aerothermal Buckling

The solution procedure using the Newton–Raphson method for the aerothermal post-buckling analysis of a functionally graded material plate is presented as follows.

Introducing the function $\{\Psi(W)\}$ to,

$$\{\Psi(W)\} = \left([K] - [K_T] + \lambda[A_a] + \frac{1}{2}[N_1] + \frac{1}{3}[N_2]\right)\{W\} - \{P_T\} = 0 \quad (9)$$

Eq. (9) can be written in the form of a truncated Taylor series expansion as

$$\{\Psi(W + \delta W)\} = \{\Psi(W)\} + \frac{d\{\Psi(W)\}}{dW}\{\delta W\} \cong 0 \quad (10)$$

Where:

$$\frac{d\{\Psi(W)\}}{dW} = [K] - [K_T] + \lambda[A_a] + \frac{1}{2}[N_1] + \frac{1}{3}[N_2] = [K_{tan}] \quad (11)$$

Thus, the Newton–Raphson iteration procedure for the determination of the post-buckling deflection can be expressed as follows:

$$\{\Psi(W)\}_i = ([K] - [K_T] + \lambda[A_a] + \frac{1}{2}([N_1])_i + \frac{1}{3}([N_2])_i)\{W\}_i - \{P_T\}$$

$$[K_{tan}]_i\{\delta W\}_{i+1} = -[K_{tan}]^{-1}\{\Psi(W)\}_i$$

$$\{W\}_{i+1} = \{W\}_i + \{\delta W\}_{i+1}$$

Convergence occurs in the preceding procedure when the maximum value of $\{\delta W\}_{i+1}$becomes less than a given tolerance $\boldsymbol{\varepsilon_{tol}}$ $(\boldsymbol{i.e.}, \mathbf{max}|\{\delta W\}_{i+1}| \boldsymbol{\varepsilon_{tol}}).[N_1] = 0$ for the symmetric geometry and deformation pattern

2.6. Panel Flutter Under Thermal Effect

In this section, the procedure of determining the critical non-dimensional dynamic pressure under the presence of thermal loading can be reduced for the solution of the linear (pre-buckling and pre-flutter) problem to the following equation:

$$[M]\{\ddot{W}\} + [G]\{\dot{W}\} + ([K] - [K_T] + \lambda[A_a] + [N_2])\{W\} = 0 \tag{12}$$

Now assume the deflection function of the transverse displacement $\{W_B\}$ to be in the form of

$$\{W_B\} = \bar{c}\{\Phi_B\}e^{\Omega t} \tag{13}$$

Where: $\Omega = \alpha + i\omega$ is the complex panel motion parameter (α is the damping ratio and ω is the frequency), $\bar{c}$ is the amplitude of vibration, and $\{\Phi_B\}$ is the mode shape.

Substituting Eq. (12) into Eq. (13), the generalized eigenvalue problem can be obtained as

$$\bar{c}[-k(M_B) + (\bar{K}_B)]\{\Phi_B\}e^{\Omega t} = \{0\} \tag{14}$$

Where: $[G_B] = \omega_0 g_a[M_B]$, and k is the non-dimensional eigenvalue given by

$$k = -\Omega^2 - \omega_0 g_a \Omega \tag{15}$$

From Eq. (14), we can write the generalized eigenvalue problem:

$$[-k(M_B) + (\bar{K}_B)]\{\Phi_B\} = \{0\} \tag{16}$$

Where: k is the eigenvalue and Φ_B is the mode shape, with the characteristic equation written as

$$|-k(M_B) + (\bar{K}_B)| = \{0\} \tag{17}$$

Given that the values of k are real for all values of below the critical value, an iterative solution can be used to determine the critical non-dimensional dynamic pressure λ_{cr}.

3. Numerical Results and Discussions

A single higher-order quadrilateral element was used to enable mesh convergence. Selecting the number of nodes per element (from 3x3 to 8x8) and integration points were progressively increased in convergence studies. The predicted post-buckling deflections and dynamic pressure responses were monitored to quantify convergence. A 5x5 node formulation with 9 Gaussian quadrature points for numerical evaluation of integrals, achieving sufficiently converged solutions. In this section, detailed numerical results and discussions are presented for the aerothermal buckling response of functionally graded square plates. The panel dimensions considered in the analysis are $1.0\ m\ x\ 1.0\ m\ x\ 0.001\ m$ the air flow and directions as showed in Figure 1. The panel is assumed to have all edges fixed. Material properties for the individual constituents are provided in Table 1. Figure 2 shows the volume fraction distributions for different cases analyzed. Each sub-plot visualizes the fraction of Aluminium and Nickel variation according to a quadratic polynomial function. Cases 1 and 2 represent homogeneous Nickel and Aluminium plates respectively.

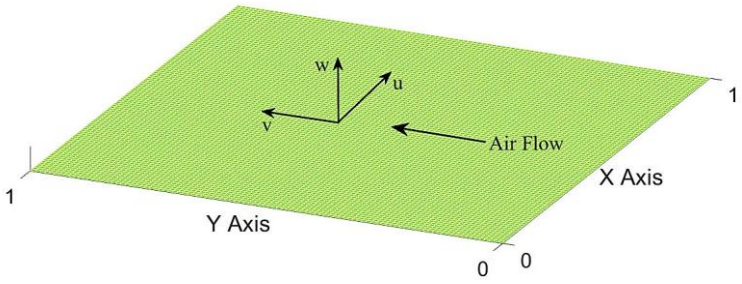

Figure 1. Schematic of Panel Geometry and Deformation.

3.1. Aerothermal Buckling Analysis

The aerothermal buckling response is evaluated for combined thermal and mechanical loading. Initially, stability boundaries are established. Subsequently, the nonlinear post-buckling behaviour is investigated for prescribed thermal loads, including temperature rise due to aerodynamic heating. The emphasis is on demonstrating the capabilities of the element with blended interpolations functions in accurately capturing complex buckling behaviour of functionally graded plates. Numerical results for stability boundaries, nonlinear deflections, and sensitivity to volume fraction variations are presented and discussed in detail. This study only includes cases where the volume fraction values ranged from 0 to 1, as volume fractions outside of this physical range were excluded.

Table 1. Mechanical and thermal properties of Ni and Al constituents

Property	Nickel	Aluminium
Modulus of Elasticity (E)	$22.4\,x10^{10}\ Pa$	$7.1\,x\,10^{10}\ Pa$
Poisson's Ratio (ν)	0.31	0.3
Thermal Expansion (α)	$9.92\,x10^{-6}\ /°C$	$22.5\,x\,10^{-6}\ /°C$
Density (ρ)	$8900\ kg/m^3$	2700 kg/m^3

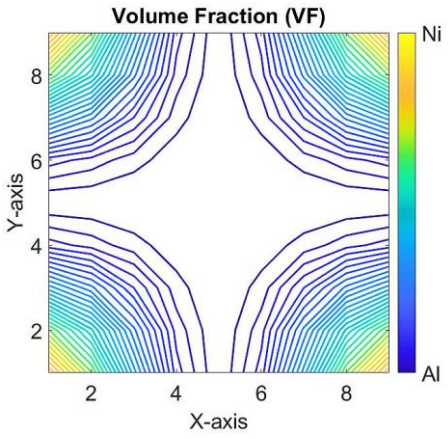

a-Case 4

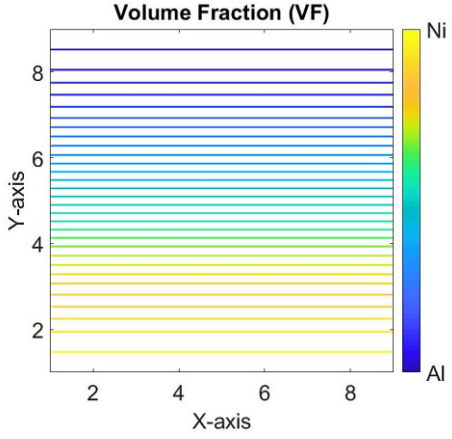

b-Case 5

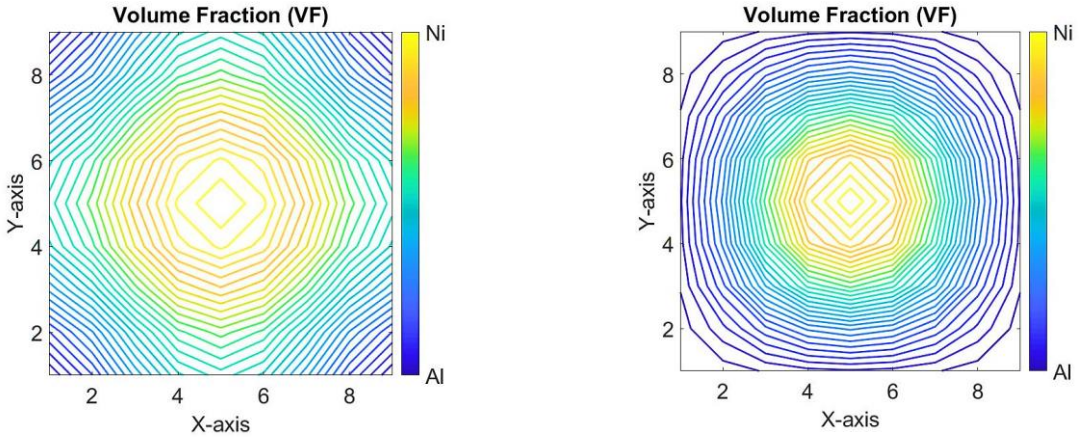

c-Case 6 **d**-Case 7

Figure 2. Identification volume fraction in contours with different Cases.

3.2. Predicting Panel Flutter Boundaries

The results in Table 2 and Figure 3 were based on using the density and flexural stiffness of the Nickel plate as reference. The initial results clearly distinguish between a plate made homogeneous Nickel (Case 1) and a plate made homogeneous Aluminium (Case 2), representing the minimum and maximum stability boundaries. A (Case 3) illustrates a 50%-50% Nickel-Aluminium composition at all points, for reference.

Placing Nickel only on the four external corners (Case 4) weakens stability improvements, as expected reduces density by 62% but decreases maximum dynamic pressure by 67% and critical buckling temperature by 54% versus the Nickel baseline. However, Placing Nickel on one entire side, with half Nickel and half Aluminium through the center and Aluminium in the opposite side (Case 5), decreases density by 35% while proportionally decreasing maximum dynamic pressure by 35% and critical buckling temperature by 39% versus full Nickel. The aligned grading a slight significantly enhances stability.

Concentrating Nickel at the mid points of the panel edges and center point (Case 6) enhances stability improvements by reduces density 23% while decreasing maximum dynamic pressure by 14% and critical buckling temperature by 23% versus Nickel. The center edge distribution provides substantial stability payoffs relative to the density reduction. Centrally locating the Nickel (Case 7) enables the highest stability improvement, decreasing density by 39% while reducing maximum dynamic pressure by 27% and critical buckling temperature by 39% relative to Nickel. The extreme concentration demonstrates the potential of tailored center-plane blending.

Table 2. Stability boundaries and Post-buckling analysis for different Cases.

	Average Density (Kg/m^3)	Maximum Dynamic Pressure ($T = 0^o$)	Critical Buckling Temperature(C)	Post-Buckling /Thickness ($T = 1.34^o$)
Case 1	8900	852	0.336	2.108
Case 2	2700	269	0.149	3.583
Case 3	5800	559	0.206	2.931
Case 4	3389	285	0.156	3.546
Case 5	5800	552	0.204	2.877
Case 6	6833	735	0.258	2.495
Case 7	5456	619	0.206	2.797

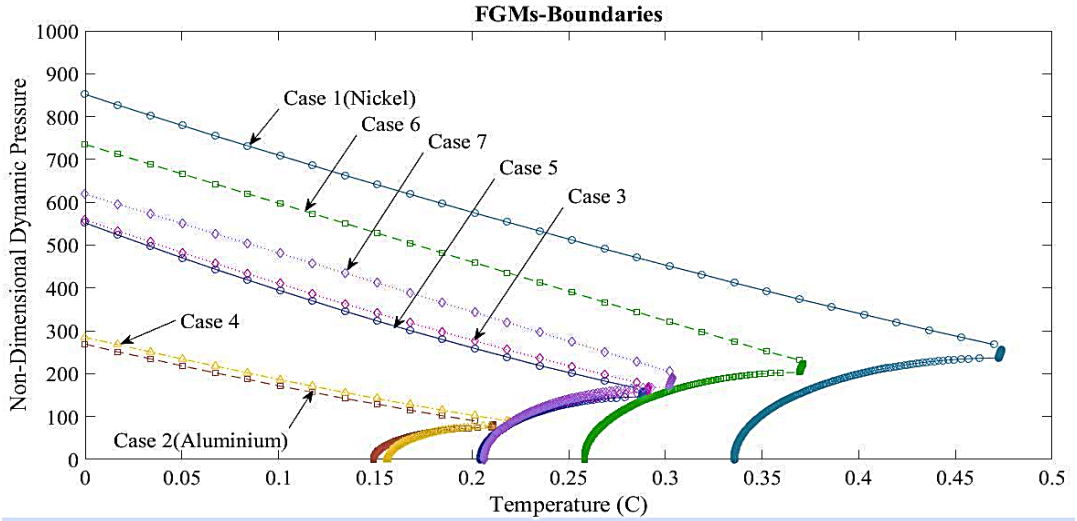

Figure 3. Stability boundaries of volume fraction distribution for different Cases.

3.3. Post-buckling deflection

The results in Table 2 and Figure 4 show nonlinear Post-buckling deflections, these results were obtained without considering dynamic pressure ($\lambda = 0$). improvement is achieved by reducing deflections. (Cases 1,2 and 3) represent the minimum and maximum Post-buckling boundaries - a fully Nickel plate, fully Aluminium plate and 50%-50% Nickel-Aluminium composition respectively.

In (Case 4), Constraining Nickel to the corners weakens Post-buckling deflections improvements, as expected increases post-buckling deflection by 68% from the Nickel baseline despite a 62% density decrease. Placing Nickel on one entire side, with half Nickel and half Aluminium through the center and Aluminium in the opposite side (Case 5) a slight significantly enhances in Post-buckling deflections, reduces density by 35% while proportionally decreasing post-buckling deflection by 36% relative to full Nickel.

Concentrating Nickel at the mid points of the panel edges and center point enhances Post-buckling deflections improvements in (Case 6) drops density 23% while limiting deflection increase to 18% over the homogeneous Nickel panel. Centrally locating the Nickel (Case 7) enables improvement in Post-buckling deflections, decreasing density 39% with a 33% post-buckling deflection increase versus the Nickel baseline. Overall, results confirm that localizing Nickel strategically in the center region of the plate with some mid-point edge optimal Post-buckling performance through deflections reduction rather than broadly distributing Nickel density.

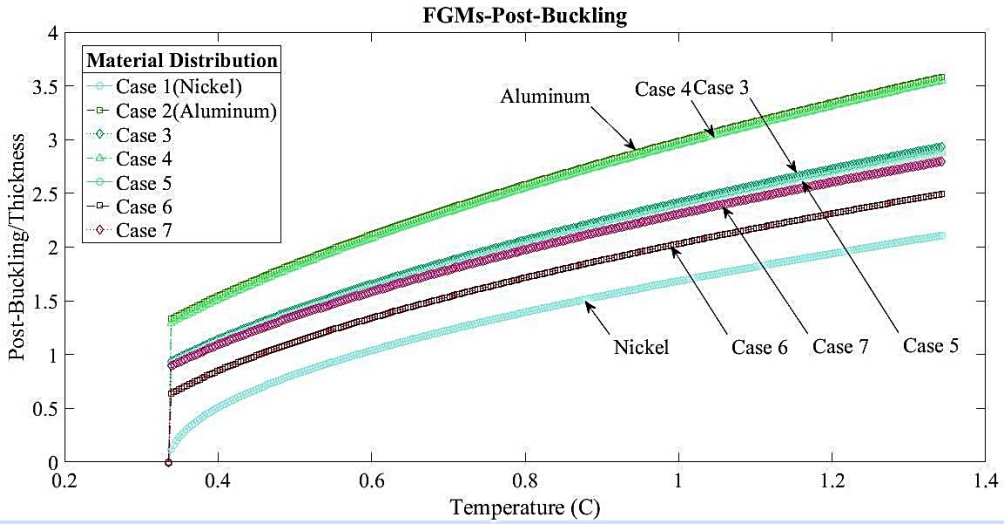

Figure 4. Post-buckling deflection / Thickness of volume fraction distribution for different Cases.

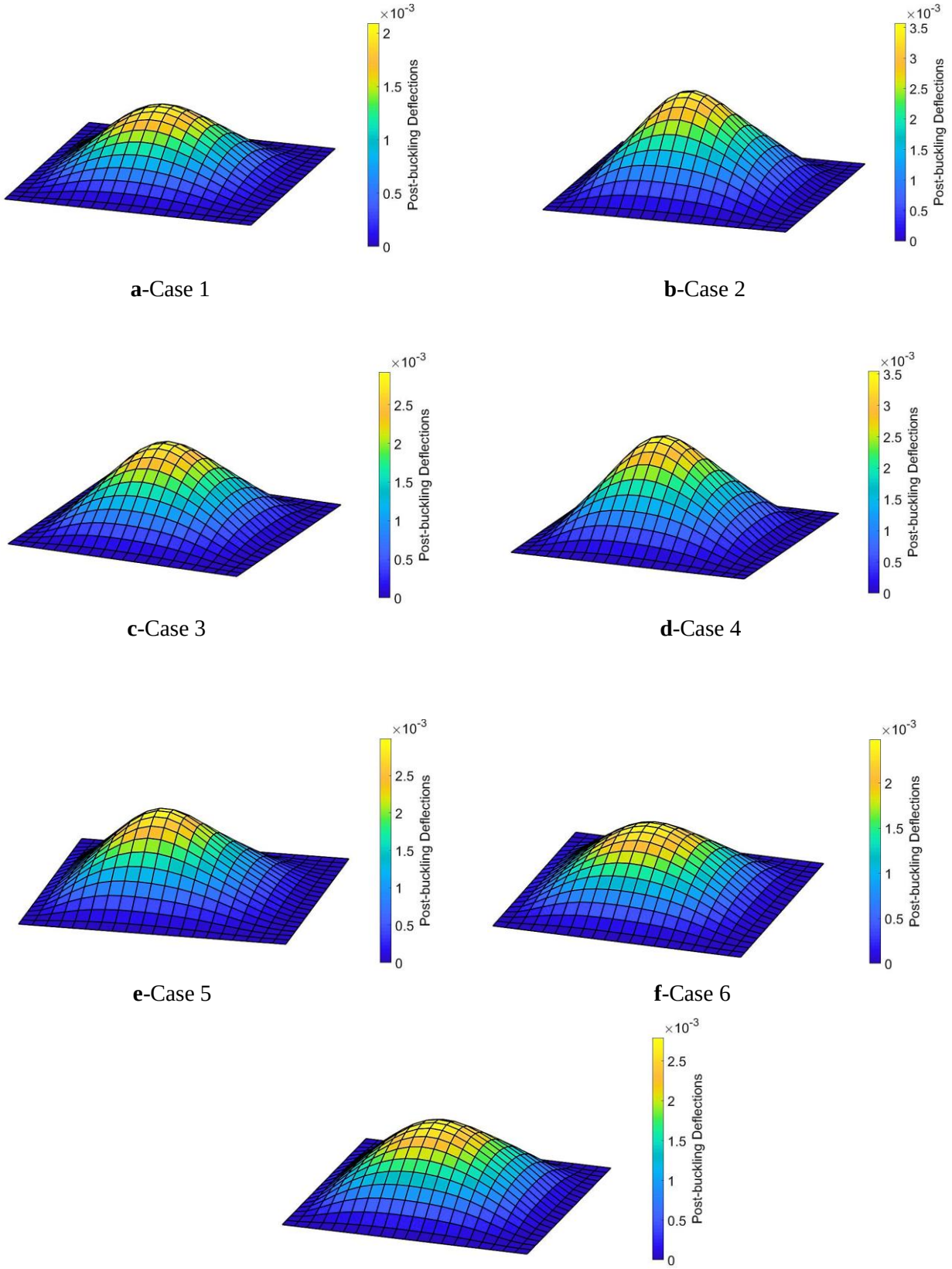

a-Case 1 **b**-Case 2

c-Case 3 **d**-Case 4

e-Case 5 **f**-Case 6

g-Case 7

Figure 5. Post-buckling deflection (m) in surface distribution for different Cases.

Figure 5 shows how the post-buckling deflections change as dynamic pressure increases ($\lambda = 150$). Case 6 and 7 have better control of deflections compared to the full Nickel panel, while their density is lower. Specifically, tailored blending in these cases increases the panel deflections by 18% and 33% respectively, for 23% and 39% less density versus full Nickel. Importantly, Case 5 with Nickel on just one side shows deflections getting much more leave for the deflections to the direction of the dynamic pressure. This indicates placing heavy material to the edges hurts stability over time even if starting deflections seem acceptable. Meanwhile, balanced central grading in Case 6 and 7 restricts growing deflections despite lowered density and pressure.

3.4. Density-Weighted Results

The initial stability analysis provided valuable insights into the effects of Nickel and Aluminium compositions on maximum dynamic pressure, critical buckling temperature, and post-buckling deflections performance. However, the density variation between Nickel and Aluminium cases complicates direct comparison between the different cases. To isolate the effects of material placement from innate density impacts, the results were dividing by density, while multiplying post-buckling deflections by density. This effectively adjusts the results for all cases to be as light as possible. The outputs allow improved evaluation of stability performance based solely on strategic material placement, excluding general density penalties or benefits as provided in Table 3.

3.4.1. Density -Weighted results by material placement

When the dynamic pressure, buckling temperature, and post-buckling deflection by density, clear placement-specific trends emerge. Regarding dynamic pressure, the highest dynamic pressure is exhibited by (Case 7) with Nickel concentrated at the center point. (Case 6) with multiple mid-point Nickel placements shows the next best performance. (Cases 2,3 and 1) comprising a full Nickel plate, 50%-50% Nickel/Aluminium mix, and full Aluminium plate respectively show similar, lower dynamic pressure. (Case 5) with Nickel on one side has comparable dynamic pressure to these lower Cases. The minimum dynamic pressure occurs with (Case 4) and Nickel only at the corners as given in Figure 6.

In terms of buckling temperature, (Case 2) with 100% Aluminium the maximum buckling temperature. (Case 4) with corner Nickel placement shows the next highest buckling. (Cases 7, 6 and 1) representing central Nickel, multi-point Nickel, and full Nickel respectively - all exhibit similar, lower buckling temperature. The minimum buckling is displayed by (Case 5 and Case 3) with side Nickel and 50%-50% material compositions as presented in Figure 7. Importantly, reducing panel density to optimize mass directly proportionally decreases the critical buckling temperature. For example, decreasing density by 25% results in a matching 25% drop in temperature stability limits. This linear coupling means density optimization inherently hamper thermal buckling.

For post-buckling deflection by density, the optimal value is achieved by the full Nickel plate in Case 1. (Cases 3, 5 and 6), covering 50% Nickel, multi-point Nickel and side Nickel arrangements all perform similarly. (Case 7) with a Nickel center point shows moderately higher deflection. (Case 4) demonstrates even higher movement with corner localization. The maximum deflection occurs with the fully Aluminium plate in (Case 2). In summary, (Cases 5,6 and7) enable weight reduction while improving post-buckling deflections over the Nickel baseline. (Cases 6 and 7) restrict deflections amplification by 18-33% despite 23-39% density decreases. Case 5 requires caution; though initial deflections improve with 35% lower density, unbalanced side placement worsens flexibility as pressures. This analysis isolates the specific positive and negative impacts of different strategic material layouts as showed in Figure 8.

Table 3. Stability boundaries and Post-buckling performance result for different Cases.

	Average Density (Kg/m^3)	$\frac{\text{Max. dyn. pressure}}{\text{Density}} * 10^3$	$\frac{\text{Crit. buck. temperature(C)}}{\text{Density}} * 10^6$	$\text{Post} - \text{Buckling /Thickness } (\text{T} = 1.34^0) * \text{Density} * 10^3$
Case 1	8900	96	38	19
Case 2	2700	100	55	10
Case 3	5800	96	36	17
Case 4	3389	84	46	12
Case 5	5800	95	35	17
Case 6	6833	108	38	17
Case 7	5456	113	38	15

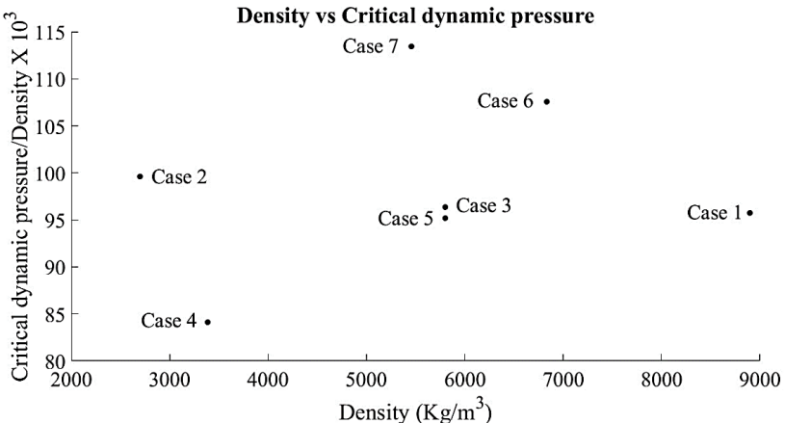

Figure 6. Non-Dimensional Dynamic pressure with density for different Cases.

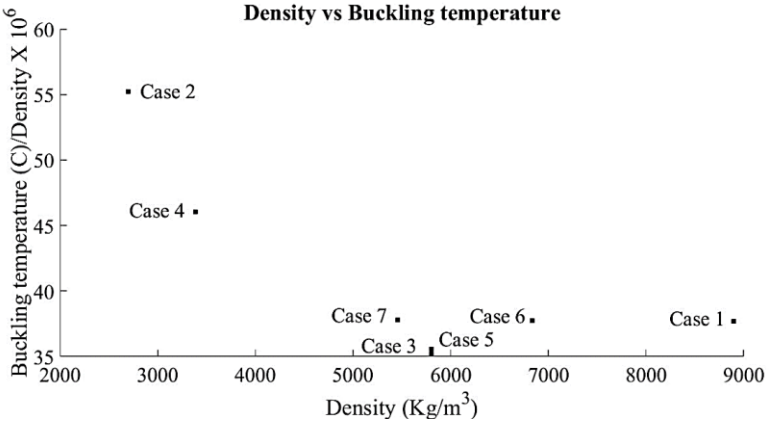

Figure 7. Buckling Temperature (C) with density for different Cases.

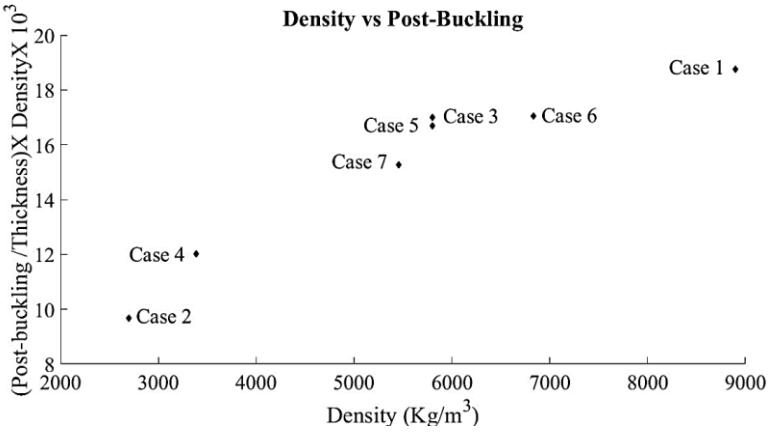

Figure 8. (Post-Buckling / Thickness) with density for different Cases.

4. Conclusion

This study demonstrates the potential for weight optimization of hypersonic panels under aero-thermal loads using tailored functionally graded Aluminium-Nickel materials. The finite element formulation enables detailed modeling of stability phenomena.

- Importantly, localizing Nickel placement at optimized center and midpoint edge locations reduces panel weight while providing optimal stability and vibration metrics when accounting for density differences.
- Specifically, concentrated Nickel at panel centers maximizes the flat zone before nonlinear deformation relative to the panel's lowered weight from mostly Aluminium composition. Though an entirely Nickel panel shows the best raw displacement reduction, targeted Nickel layouts offer the most gains per unit mass reduction.
- Corner Nickel concentrations conversely weaken stability for their weight fraction. Intermediate side Nickel augmentation provides moderate performance per density trade-offs.
- Overall, tailored Nickel localization strategies can substantially enhance panel dynamic pressure and post-buckling deflections behaviors through placement at optimal centers and midpoints without significantly increasing thickness and mass.
- Importantly, reducing panel density directly causes a proportional decrease in critical buckling temperature. This coupling means density optimizations inherently hamper thermal buckling performance.

In summary, placing heavier constituents at optimal graded locations allows the stiffening benefits to outweigh diminished inertia and rigidity from overall density declines. The balanced localized approach may support developing damage tolerant hypersonic panels which meet simultaneous dynamic pressure and post-buckling deflections.

5. Future Work

An area of recommended future effort involves expanding the volume fraction representation to higher order polynomial variations beyond the current quadratic approximation. Implementing cubic or higher polynomials can enable modeling more complex and smoother material gradations across the panel plane. The investigation would specifically analyze the impacts of elevating the volume fraction variation order on the resulting buckling temperature response. Smoothness of the structural gradients can potentially improve thermal stability limits in addition to vibration metrics. Additionally, the authors plan to leverage the modeling capabilities established in the presented study to implement optimization techniques for stability and weight metrics in future work.

6. References

[1] H. H. Ibrahim, M. Tawfik, and M. Al-Ajmi 2007 Thermal Buckling and Nonlinear Flutter Behavior of Functionally Graded Material Panels *Journal of Aircraft* vol. 44 no. 5 pp. 1610-1618.
[2] H. H. Ibrahim, M. Tawfik, and M. Al-Ajmi 2007 Non-linear panel flutter for temperature-dependent functionally graded material panels *Computational Mechanics* vol. 41 no. 2 pp. 325-334.
[3] A. Shaker, W. Abdelrahman, M. Tawfik, and E. Sadek 2008 Stochastic Finite element analysis of the free vibration of functionally graded material plates *Computational Mechanics* vol. 41 no. 5 pp. 707-714.
[4] K. J. Sohn and J. H. Kim 2009 Nonlinear thermal flutter of functionally graded panels under a supersonic flow *Composite Structures* vol. 88 no. 3 pp. 380-387.
[5] I. Hesham Hamed and M. Tawfik 2010 Limit-cycle Oscillations of Functionally Graded Material Plates Subject to Aerodynamic and Thermal Loads *Journal of Vibration and Control* vol. 16 no. 14 pp. 2147-2166.
[6] H. H. Ibrahim, H. H. Yoo, M. Tawfik, and K.-S. Lee 2010 Thermo-acoustic random response of temperature-dependent functionally graded material panels *Computational Mechanics* vol. 46 no. 3 pp. 377-386.
[7] L. V. Tran, C. H. Thai, and H. Nguyen-Xuan 2013 An isogeometric finite element formulation for thermal buckling analysis of functionally graded plates *Finite Elements in Analysis and Design* vol. 73 pp. 65-76.
[8] A. H. Taheri, B. Hassani, and N. Z. Moghaddam 2014 Thermo-elastic optimization of material distribution of functionally graded structures by an isogeometrical approach *International Journal of Solids and Structures* vol. 51 no. 2 pp. 416-429.
[9] T. Xiang, S. Natarajan, H. Man, C. Song, and W. Gao 2014 Free vibration and mechanical buckling of plates with in-plane material inhomogeneity – A three dimensional consistent approach *Composite Structures* vol. 118 pp. 634-642.
[10] L. W. Zhang, P. Zhu, and K. M. Liew 2014 Thermal buckling of functionally graded plates using a local Kriging meshless method *Composite Structures* vol. 108 pp. 472-492.
[11] L. Li and D. G. Zhang 2016 Free vibration analysis of rotating functionally graded rectangular plates *Composite Structures* vol. 136 pp. 493-504.
[12] Q. X. Lieu, S. Lee, J. Kang, and J. Lee 2018 Bending and free vibration analyses of in-plane bi-directional functionally graded plates with variable thickness using isogeometric analysis *Composite Structures* vol. 192 pp. 434-451.
[13] K. Khorshidi and M. Karimi 2019 Flutter analysis of sandwich plates with functionally graded face sheets in thermal environment *Aerospace Science and Technology* vol. 95.
[14] E. Ansari and A. Setoodeh 2020 Applying isogeometric approach for free vibration, mechanical, and thermal buckling analyses of functionally graded variable-thickness blades *Journal of Vibration and Control* vol. 26 no. 23-24 pp. 2193-2209.
[15] A. Muc and J. Flis 2021 Flutter characteristics and free vibrations of rectangular functionally graded porous plates *Composite Structures* vol. 261.
[16] Y. Sun, Z. Song, W. Ma, and F. Li 2021 Influence mechanism of lumped masses on the flutter behavior of structures *Aerospace Science and Technology* vol. 111.
[17] W. Tian, T. Zhao, Y. Gu, and Z. Yang 2022 Nonlinear flutter suppression and performance evaluation of periodically embedded nonlinear vibration absorbers in a supersonic FGM plate *Aerospace Science and Technology* vol. 121.
[18] S. Zhong, G. Jin, T. Ye, and Q. Zhang 2022 Supersonic flutter analysis of variable thickness blades in thermal environment by using isogeometric approach *Thin-Walled Structures* vol. 172.
[19] H. Guo, K. K. Żur, and X. Ouyang 2023 New insights into the nonlinear stability of nanocomposite cylindrical panels under aero-thermal loads *Composite Structures* vol. 303.
[20] P. Li, Z. Yang, and W. Tian 2023 Nonlinear aeroelastic analysis and active flutter control of functionally graded piezoelectric material plate *Thin-Walled Structures* vol. 183.

[21] J. Liu, Y. Zhang, Y. Zhang, S. Kitipornchai, and J. Yang 2023 Aeroelastic analyses of functionally graded aluminium composite plates reinforced with graphene nanoplatelets under fluid-structural interaction *Aerospace Science and Technology* vol. 136.
[22] M. Zanjanchi, M. Ghadiri, and S. Sabouri-Ghomi 2023 Dynamic stability and bifurcation point analysis of FG porous core sandwich plate reinforced with graphene platelet *Acta Mechanica* vol. 234 no. 10 pp. 5015-5037.
[23] W. Zhang, C. Wang, and Y. Wang 2023 Thermo-mechanical analysis of porous functionally graded graphene reinforced cylindrical panels using an improved third order shear deformable model *Applied Mathematical Modelling* vol. 118 pp. 453-473.
[24] M. Tawfik 2018 In Search for the Super Element:Algorithms to Generate HigherOrder Elements *ResearchGate* [Online] DOI: 10.31142/ijtsrd18565.
[25] M. Tawfik 2021 Panel Flutter *ResearchGate* [Online] DOI:10.13140/RG.2.1.1537.6807.